Int. J. Electron. Commun. (AEÜ) 83 (2018) 359–365

Contents lists available at ScienceDirect

Int. J. Electron. Commun. (AEÜ)

journal homepage: www.elsevier.com/locate/aeue

Regular paper

Joint angular and spectral estimation technique using nonlinear Kalman filters for cognitive radio

Samar Elaraby[a,*], Heba Y. Soliman[a], Heba M. Abdel-Atty[a], Mohamed A. Mohamed[b]

[a] Faculty of Engineering, Port Said University, Port Said, Egypt
[b] Faculty of Engineering, Mansoura University, Mansoura, Egypt

ARTICLE INFO

Keywords:
DOA estimation
Spectrum sensing
Kalman filter
EKF
UKF
Cognitive radio

ABSTRACT

The joint estimation of direction of arrivals (DOA) and carrier frequencies of band-limited source signals is considered in this paper. A novel technique based on nonlinear Kalman filters is proposed for this joint angular and spectral estimation problem for cognitive radio (CR). Since sampling a wideband spectrum at Nyquist rate increases the analog-to-digital converter (ADC) requirements, we propose executing Kalman filter algorithm over a spatial state space model. Thus, one time sample is required and hardware complexity is reduced. Two types of nonlinear Kalman filters, extended Kalman filter (EKF) and unscented Kalman filter (UKF), are proposed. We consider their sub-optimal performance and show how to control their convergence. However, the proposed algorithms can detect a number of source signals limited to the number of elements in employing arrays.

1. Introduction

Today, radio applications encounter a lack of frequency resources due to the dramatic increase in radio devices. To overcome this problem, CR has been introduced in [1]. CR aims to efficiently exploit the licensed spectrum without interfering the transmissions of the licensed users. Thus, secondary users (SUs) opportunistically access licensed frequency bands left vacant by their own primary users (PUs). Then, SU has to continuously detect unoccupied frequency channels over a wideband spectrum even after it has been assigned to unoccupied bands. The reason is that SUs have to free the frequency band as soon as the PU shows up over the channel. As a result, wideband spectrum sensing has gained great attention in the last decade. Many proposals have been presented in the literature to tackle spectrum sensing and its associated problems for CR as in [2,3]. The main problem facing wideband spectrum sensing is the need to sample a wideband spectrum. Since the SU has to scan a wideband spectrum simultaneously, it should sample the wideband received signals at high Nyquist rates. As a result, high-speed analog-to-digital converters (ADCs) are required in the front-ends of SUs. Thus, sub-Nyquist sampling proposals have been introduced to spectrum sensing to relax the ADC requirements. However, the main challenge is that sub-Nyquist sampling requires employing a large number of relaxed ADCs.

Furthermore, the advances in CR technology take the advantages of the spatial domain as well. SU can share the same band frequency with PU in the same time and in the same area if they transmit their signals in two different directions. As a result, DOA estimation becomes a vital process for spectrum sensing. One of the main factors that evaluate the performance of DOA estimation is the degrees of freedom as the higher the degrees of freedom, the more the number of PUs can be detected. This, in turn, increases the spatial capacity of CR. Many state-of-the-art methods have handled the problem of achieving higher degrees of freedom using sparse arrays. Recently, the authors in [4,5] have exploited co-prime arrays for this purpose. The conformal array has also been used in [6,7]. Moreover, 2D-DOA has been also investigated to increase the spatial capacity as in [8,9].

The problem of jointly estimating carrier frequencies and their corresponding DOAs has been addressed in the literature. In [10–12], the authors have proposed their methods at Nyquist sampling rate. Recently, sub-Nyquist methods have gained more attention, and many proposals have been presented. In [13–15], the authors have implemented sub-Nyquist sampling using delayed paths connected in parallel to the direct paths after the array elements. Each delayed path has its own relaxed ADC to perform sub-Nyquist sampling. Then, algorithms, like ESPRIT [16] and MUSIC [17], have been used to detect both the carrier frequency and corresponding DOA of PUs. Although these proposals succeeded in relaxing the sampling rate, they had to employ a large number of ADCs. Besides, the degrees of freedom are restricted to the number of the employed array elements. On the other hand, other proposals have given their attention to increase the degrees of freedom. A 2D nested array has been exploited in [18] to increase the degrees of freedom. However, a minimum redundancy linear array has

* Corresponding author.
E-mail addresses: samar.elaraby@eng.psu.edu.eg (S. Elaraby), hebayms1@yahoo.com (H.Y. Soliman), heba_atty@ieee.org (H.M. Abdel-Atty), mazim12@yahoo.com (M.A. Mohamed).

http://dx.doi.org/10.1016/j.aeue.2017.10.007
Received 27 February 2017; Accepted 6 October 2017

been employed for the same purpose in [19]. The authors of [20] have proposed exploiting a standard uniform rectangular array (URA) with delay channels to enhance its degrees of freedom. Besides, the authors have detected 2D-DOA instead of a single DOA to increase the spatial capacity. Although all the proposals in [18–20] have accomplished higher degrees of freedom, all of them still need a large number of relaxed ADCs to execute sub-Nyquist sampling.

In this paper, a novel approach based on nonlinear Kalman filters is proposed for solving the problem of jointly estimating carrier frequencies and their corresponding DOAs for CR. In contrast to the aforementioned methods, we focus on reducing the hardware complexity of the considered problem. For this purpose, we investigate the spatial domain using Kalman filter (KF) to detect both the carrier frequencies and their corresponding DOAs of PUs. As a result, one time sample at each array element is required leading to reducing the required sampling rate, and hence it reduces the hardware requirements. In fact, a number of ADCs equal to the employed array elements are sufficient to sample the signal at a relaxed sampling rate. Since there is no need to reconstruct the spectrum itself in the considered problem, the relaxed sampling rate has no restrictions. On the other hand, we rely on an L-shaped uniform array to form a spatial state space. Since the L-shaped array is a dense array, the degrees of freedom of our proposal are restricted by the number of array elements. However, the L-shaped array gives SUs the capability to detect all the directions of the plane of SU, in contrast to a single ULA. Two different algorithms are proposed based on two different types of nonlinear Kalman filters. The first filter is extended Kalman filter (EKF) [21] and the second is unscented Kalman filter (UKF) [22]. Using simulations, we investigate the issues that affect the sub-optimal performance of both of them.

The rest of the paper is organized as follows. Section 2 describes the L-shaped array model employed and states the problem being considered. Kalman filter is then visited in Section 3 to emphasize its main concept. The proposed spatial state space model is derived and followed by a description of both EKF-based and UKF-based approaches in Section 4. The simulation results with comparative study are presented in Section 5. Finally, Section 6 derives conclusions.

2. Preliminaries

2.1. System model

Consider two ULAs connected together to form an L shape. The first array is located on the x-axis and the other one is on the z-axis. Each array has N elements including the connecting one located on the corner of the L shape, i.e., the whole number of elements is $2N-1$. The connecting element is considered as a reference point for both two arrays. Suppose L uncorrelated band-limited source signals are transmitted on separate carrier frequencies. The source signals are incident on the arrays with different DOAs. Thus, each element in both two arrays receives delayed versions of the source signals received by the reference point. Then, the output at the nth element in the x-array and the z-array respectively is defined by

$$\begin{aligned} y_x^n(t) &= \sum_{l=1}^{L} s_l(t) e^{-j2\pi(n-1)d\frac{\sin\theta_l}{\lambda_l}} + \eta_x^n(t) \\ y_z^n(t) &= \sum_{l=1}^{L} s_l(t) e^{-j2\pi(n-1)d\frac{\cos\theta_l}{\lambda_l}} + \eta_z^n(t) \end{aligned} \tag{1}$$

where $s_l(t)$, with $l = 1,2...L$, denotes the signal transmitted from lth source and arrives the two arrays with a wavelength of λ_l and a direction of arrival of θ_l. The element spacing in both two arrays is denoted as d. In addition, $\eta_x^n(t)$ and $\eta_z^n(t)$ denote noise signals in the nth element of the x-array and the z-array respectively. Both $\eta_x^n(t)$ and $\eta_z^n(t)$ are assumed to be complex Gaussian white noise with zero mean and variance of σ_n^2.

2.2. Problem statement

In cognitive radio, SUs do not have any prior information about PUs being detected. The number of PUs is even unknown, and then SUs have to blindly detect carrier frequencies and their corresponding DOAs. Thus, the problem being solved in this paper is to find both the carrier frequency and DOA for every PU source signal that arrives the arrays, while the measured outputs at the two arrays are the only known information.

We propose nonlinear KFs for blindly estimating $\frac{\sin\theta_l}{\lambda_l}$ and $\frac{\cos\theta_l}{\lambda_l}$ pairs using a state space model derived from Eq. (1). Then, carrier frequencies and DOAs can be evaluated. The main concept of KFs is going to be discussed in the next section, before a detailed analysis of our proposal is presented in Section 4.

3. Kalman filters: An overview

KF is a recursive algorithm used to estimate the state variable $\mathbf{x} \in \mathbb{R}^M$ from a state space model depending on noisy measurements. The state space model consists of process model that derives a relation between any two successive states of the system, and measurement model that represents the relation between the measurements and the state variable. A linear state space model is described as

$$\begin{aligned} \mathbf{x}_{k+1} &= \mathbf{A}_k\mathbf{x}_k + \mathbf{w}_k \\ \mathbf{y}_k &= \mathbf{H}\mathbf{x}_k + \mathbf{u}_k \end{aligned} \tag{2}$$

where $\mathbf{x}_{k+1}$ and $\mathbf{x}_k$ denote posterior and prior state variables respectively. The matrices $\mathbf{A}_k$ and $\mathbf{H}$ represent the transition matrix and the observation matrix respectively. However, $\mathbf{w}_k$ and $\mathbf{u}_k$ respectively denote process noise and measurements noise, which are assumed to be Gaussian distributed with zero mean and covariance of $\mathbf{Q}$ and $\mathbf{R}$ respectively. The process noise covariance matrix $\mathbf{Q}$ represents uncertainty in the state space model. However, the measurements noise covariance matrix $\mathbf{R}$ represents uncertainty in measurements.

KF algorithm has two steps, prediction step and updating step. In prediction step, the filter predicts statistics of the posterior state from the previous one. In updating step, the predicted estimates are corrected depending on observed measurements. KF is an optimal filter that converges to optimal solutions. Since nonlinear systems cannot fit the linear combinations in Eq. (2), traditional KF cannot be employed on nonlinear systems. So modified KFs are derived to handle nonlinear state space models. Two of the renowned nonlinear Kalman filters are EKF and UKF.

In EKF, the nonlinear state space model is linearized using Taylor series and approximated to the first order derivatives. However, approximation leads to accumulative errors in the estimates through iterations. Thus, EKF is considered as a sub-optimal filter, which may diverge. On the other hand, UKF depends on unscented transformation. The filter captures the statistics of the state variable using sample points. Sample points are then propagated through the system while keeping the true statistics of the state variable. From the transferred sample points, the state variable can be reconstructed at the output of the system. UKF is accurate to the third order partial derivatives and considered as a sub-optimal filter as well. This, in turn, leads to a better performance than EKF. We propose using both EKF and UKF for the estimation problem considered in this paper. Readers can refer to [21,22] for detailed descriptions of EKF and UKF algorithms respectively.

4. Proposed approaches

In this section, we present our proposed work. First, the proposed spatial state space is derived from Eq. (1). Then, two approaches are proposed using EKF and UKF respectively.

4.1. State space formulation

Each source signal is exposed to the same time delay between any two successive elements in the array. The lth source signal that reaches the $(n+1)$th element of both two arrays X_l^{n+1} and Z_l^{n+1} can be determined from its version at the previous element X_l^n and Z_l^n respectively

$$X_l^{n+1} = e^{-j2\pi d\frac{\sin\theta_l}{\lambda_l}} X_l^n$$
$$Z_l^{n+1} = e^{-j2\pi d\frac{\cos\theta_l}{\lambda_l}} Z_l^n \tag{3}$$

Eq. (3) obviously represents a state space model in the spatial domain. Exploiting the spatial domain gives an advantage over the temporal state space, as there is no need to capture more than one time sample. Consequently, there is no need to use high-speed ADCs in capturing wideband spectrum. In other words, the proposed sensing technique in this paper can still successfully detect a wideband spectrum without requiring any additional hardware complexity.

Both X_l^{n+1} and Z_l^{n+1}, where $l = 1,...L$, are complex signals, so each one can be decomposed into two real variables that represent the real and imaginary parts. Suppose $X_l^{n+1} = x_{2l-1}^{n+1} + jx_{2l}^{n+1}$ and $Z_l^{n+1} = z_{2l-1}^{n+1} + jz_{2l}^{n+1}$. Then, Eq. (3) can be redefined as

$$\begin{bmatrix} x_{2l-1}^{n+1} \\ x_{2l}^{n+1} \end{bmatrix} = \begin{bmatrix} \cos\left(2\pi d\frac{\sin\theta_l}{\lambda_l}\right) & \sin\left(2\pi d\frac{\sin\theta_l}{\lambda_l}\right) \\ -\sin\left(2\pi d\frac{\sin\theta_l}{\lambda_l}\right) & \cos\left(2\pi d\frac{\sin\theta_l}{\lambda_l}\right) \end{bmatrix} \begin{bmatrix} x_{2l-1}^n \\ x_{2l}^n \end{bmatrix} \tag{4}$$

$$\begin{bmatrix} z_{2l-1}^{n+1} \\ z_{2l}^{n+1} \end{bmatrix} = \begin{bmatrix} \cos\left(2\pi d\frac{\cos\theta_l}{\lambda_l}\right) & \sin\left(2\pi d\frac{\cos\theta_l}{\lambda_l}\right) \\ -\sin\left(2\pi d\frac{\cos\theta_l}{\lambda_l}\right) & \cos\left(2\pi d\frac{\cos\theta_l}{\lambda_l}\right) \end{bmatrix} \begin{bmatrix} z_{2l-1}^n \\ z_{2l}^n \end{bmatrix} \tag{5}$$

Thus, the state variable $\mathbf{x}_s \in \mathbb{R}^{4L\times 1}$ is formed at any element as a concatenation of the real and imaginary parts of the L source signals that arrive this element in the x-array followed by their versions arrive the corresponding z-array element, i.e., $\mathbf{x}_s = [\mathbf{x}_r\ \mathbf{z}_r]^T$ where $\mathbf{x}_r = [x_1\ x_2\ ...\ x_{2L-1}\ x_{2L}]^T$ and $\mathbf{z}_r = [z_1\ z_2\ ...\ z_{2L-1}\ z_{2L}]^T$.

While Kalman filter is going to predict the posterior state variable in the spatial domain, it is assumed to predict the unknown DOAs and carrier frequencies as well. So the state variable expands to contain these parameters. Thus, the state variable becomes $\mathbf{x}_s = [\mathbf{x}_r\ \mathbf{z}_r\ \mathbf{A}\ \mathbf{B}]^T$ where $\mathbf{x}_s \in \mathbb{R}^{6L\times 1}$ and the column vectors $\mathbf{A}$ and $\mathbf{B}$ are described as

$$\mathbf{A} = [A_1\ ...\ A_L]^T = \left[\frac{\sin\theta_1}{\lambda_1}\ ...\ \frac{\sin\theta_L}{\lambda_L}\right]^T$$
$$\mathbf{B} = [B_1\ ...\ B_L]^T = \left[\frac{\cos\theta_1}{\lambda_1}\ ...\ \frac{\cos\theta_L}{\lambda_L}\right]^T \tag{6}$$

The reason of selecting $\frac{\sin\theta_l}{\lambda_l}$ and $\frac{\cos\theta_l}{\lambda_l}$ instead of directly selecting θ_l and λ_l as state parameters is discussed later in Section 4.2. Now, the process model of the spatial state space model can be formed

$$\mathbf{x}_s^{n+1} = \begin{bmatrix} \boldsymbol{\alpha}_x & 0 & 0 & 0 \\ 0 & \boldsymbol{\alpha}_z & 0 & 0 \\ 0 & 0 & \mathbf{I} & 0 \\ 0 & 0 & 0 & \mathbf{I} \end{bmatrix} \mathbf{x}_s^n \tag{7}$$

where $\mathbf{I} \in \mathbb{R}^{L\times L}$ is the identity matrix. The matrices $\boldsymbol{\alpha}_x$ and $\boldsymbol{\alpha}_z \in \mathbb{R}^{2L\times 2L}$ are defined as

$$\boldsymbol{\alpha}_x = \begin{bmatrix} \boldsymbol{\alpha}_{x1} & 0 & 0 \\ 0 & \ddots & 0 \\ 0 & 0 & \boldsymbol{\alpha}_{xL} \end{bmatrix}$$
$$\boldsymbol{\alpha}_z = \begin{bmatrix} \boldsymbol{\alpha}_{z1} & 0 & 0 \\ 0 & \ddots & 0 \\ 0 & 0 & \boldsymbol{\alpha}_{zL} \end{bmatrix} \tag{8}$$

where

$$\boldsymbol{\alpha}_{xl} = \begin{bmatrix} \cos\left(2\pi d\frac{\sin\theta_l}{\lambda_l}\right) & \sin\left(2\pi d\frac{\sin\theta_l}{\lambda_l}\right) \\ -\sin\left(2\pi d\frac{\sin\theta_l}{\lambda_l}\right) & \cos\left(2\pi d\frac{\sin\theta_l}{\lambda_l}\right) \end{bmatrix}$$
$$\boldsymbol{\alpha}_{zl} = \begin{bmatrix} \cos\left(2\pi d\frac{\cos\theta_l}{\lambda_l}\right) & \sin\left(2\pi d\frac{\cos\theta_l}{\lambda_l}\right) \\ -\sin\left(2\pi d\frac{\cos\theta_l}{\lambda_l}\right) & \cos\left(2\pi d\frac{\cos\theta_l}{\lambda_l}\right) \end{bmatrix} \tag{9}$$

with $l = 1,2,...L$.

The second equation forms the state space model is the measurement model. The measurement model represents the output of the nth element in both two arrays. The real and imaginary parts of the output of the nth element in the x-array can be deduced as

$$Y_{x,re}^n = \sum_{l=1}^{L} x_{2l-1}^n + u_{x,re}^n$$
$$Y_{x,im}^n = \sum_{l=1}^{L} x_{2l}^n + u_{x,im}^n \tag{10}$$

where $u_{x,re}^n$ and $u_{x,im}^n$ are the real and imaginary parts of Gaussian white noise signal η_x^n. The same is applied to the z-array. Thus, the measurement model in matrix notation becomes

$$\mathbf{Y}_n = [Y_{x,re}^n\ Y_{x,im}^n\ Y_{z,re}^n\ Y_{z,im}^n]^T = \begin{bmatrix} 1 & 0 & & 1 & 0 & 0 & 0 & & 0 & 0 & 0 & & 0 \\ 0 & 1 & & 0 & 1 & 0 & 0 & & 0 & 0 & 0 & & 0 \\ 0 & 0 & ... & 0 & 0 & 1 & 0 & ... & 1 & 0 & 0 & ... & 0 \\ 0 & 0 & & 0 & 0 & 0 & 1 & & 0 & 1 & 0 & & 0 \end{bmatrix} \mathbf{x}_s^n + \mathbf{u}_n \tag{11}$$

The nonlinear process model and the linear measurements model in Eqs. (7) and (11) respectively can be gathered in a state space model like the one described in Eq. (2)

$$\mathbf{x}_s^{n+1} = f(\mathbf{x}_s^n)$$
$$\mathbf{Y}_n = \mathbf{H}\,\mathbf{x}_s^n + \mathbf{u}_n \tag{12}$$

where $f(.)$ is the nonlinear function that represents the system, $\mathbf{H}$ is the observation matrix with $\mathbf{H} \in \mathbb{R}^{4\times 6L}$ and $\mathbf{u}_n$ represents measurements noise where $\mathbf{u}_n \sim N(0,\mathbf{R})$. The measurements noise covariance matrix $\mathbf{R}$ represents uncertainty in measurements due to noise signals. However, the process noise covariance matrix $\mathbf{Q}$ is set to be zero giving full trust in the proposed state space model. Since the state space model represents a nonlinear system, traditional linear Kalman filter would be inefficient at evaluating optimal estimate. Thus, sub-optimal EKF and UKF are recommended to deal with nonlinearity in this problem.

4.2. Proposed extended Kalman filter-based approach

EKF linearizes the nonlinear system about the estimated trajectory. The linearization is performed using Taylor series and approximated to the first order partial derivatives along the trajectory. This, in turn, leads to degraded accuracy for strong nonlinear systems. Since the filter updates the estimated trajectory every iteration depending on measurements, the partial derivatives, in turn, follow observed measurements. As a result, EKF is exposed to tremendous errors caused by linearization approximation and the influence of noisy measurements on partial derivatives. The errors accumulate over iterations and eventually lead the filter to diverge.

Since EKF is a sub-optimal filter and may fail to converge to the true values, we propose a way for encouraging the filter to converge to the true carrier frequencies and DOAs. The parameters to be estimated are selected to have small variances relative to a region where the system is relatively linear. Since the state parameters are supposed to relate to the carrier frequencies and DOAs and have small variances as well, the parameters $\frac{\sin\theta_l}{\lambda_l}$ and $\frac{\cos\theta_l}{\lambda_l}$ are selected as stated in Eq. (6). These parameters range between 1 and -1, and then they help the filter to search

over a small region more quickly and efficiently. Besides, reducing the inter-element spacing d of the employed array leads to expand the sinusoidal process model, Eqs. (4) and (5), regarding to the unknown parameters. Then, the filter tends to search for the unknown parameters over a small range that is relatively linear resulting in a dramatic performance improvement. Moreover, initializing EKF with a value close to the mean value of the state parameters encourages the filter to operate in the target linear range and converge to the true values with reasonable errors. Besides, tuning the filter with selecting a suitable $\mathbf{R}$ leads to overcome the effect of noisy measurements. As a result, EKF tends to approach the performance of traditional KF under these conditions.

Now, EKF can be applied to the state space model described in Eqs. (7) and (11) to estimate the state variable $\mathbf{x}_s$. First, EKF is initialized with the initial estimate $\hat{\mathbf{x}}_0 = \mathrm{E}[\mathbf{x}_s]$ and initial covariance matrix $\mathbf{P}_0 = \mathrm{E}[(\mathbf{x}_s - \hat{\mathbf{x}}_0)(\mathbf{x}_s - \hat{\mathbf{x}}_0)^T]$. Then, it predicts the posterior estimates $\hat{\mathbf{x}}_n^-$ and its covariance matrix $\mathbf{P}_n^-$ from the previous state. The filter finally updates the estimates depending on observed measurements at the array elements. The filter goes through multiple iterations till the filter convergence. Every iteration consists of two steps as follows.

4.2.1. Prediction step

The posterior estimates $\hat{\mathbf{x}}_n^-$ and covariance matrix $\mathbf{P}_n^-$ are predicted as described in [21] with

$$\begin{aligned}\hat{\mathbf{x}}_n^- &= f(\hat{\mathbf{x}}_{n-1})\\ \mathbf{P}_n^- &= \mathbf{F}_n \mathbf{P}_{n-1} \mathbf{F}_n^T\end{aligned} \tag{13}$$

where $\mathbf{F}_n$ is Jacobian matrix of $f(.)$ and contains the first order partial derivatives of $f(x_s^n)$.

$$\mathbf{F}_n = \frac{\partial f(\mathbf{x}_s^{n-1})}{\partial \mathbf{x}_s^{n-1}}\Big|_{\mathbf{x}_s^{n-1}=\hat{\mathbf{x}}_{n-1}} = \begin{bmatrix} \mathbf{f}_1 & 0 & \mathbf{f}_3 & 0 \\ 0 & \mathbf{f}_2 & 0 & \mathbf{f}_4 \\ 0 & 0 & \mathbf{I} & 0 \\ 0 & 0 & 0 & \mathbf{I} \end{bmatrix} \tag{14}$$

where $\mathbf{I} \in \mathbb{R}^{L\times L}$ is the identity matrix. $\mathbf{f}_1$,$\mathbf{f}_2$,$\mathbf{f}_3$ and $\mathbf{f}_4$ are defined as follows

$$\begin{aligned}\mathbf{f}_1 &= \begin{bmatrix} \ddots & 0 & 0 \\ 0 & \boldsymbol{\beta}_{1l} & 0 \\ 0 & 0 & \ddots \end{bmatrix}, \quad \mathbf{f}_2 = \begin{bmatrix} \ddots & 0 & 0 \\ 0 & \boldsymbol{\beta}_{2l} & 0 \\ 0 & 0 & \ddots \end{bmatrix}\\ \mathbf{f}_3 &= \begin{bmatrix} \ddots & 0 & 0 \\ 0 & \boldsymbol{\beta}_{3l} & 0 \\ 0 & 0 & \ddots \end{bmatrix}, \quad \mathbf{f}_4 = \begin{bmatrix} \ddots & 0 & 0 \\ 0 & \boldsymbol{\beta}_{4l} & 0 \\ 0 & 0 & \ddots \end{bmatrix}, \quad l = 1,2,...L\end{aligned} \tag{15}$$

$$\boldsymbol{\beta}_{1l} = \begin{bmatrix} \frac{\partial x_{2l-1}^n}{\partial x_{2l-1}^{n-1}} & \frac{\partial x_{2l-1}^n}{\partial x_{2l}^{n-1}} \\ \frac{\partial x_{2l}^n}{\partial x_{2l-1}^{n-1}} & \frac{\partial x_{2l}^n}{\partial x_{2l}^{n-1}} \end{bmatrix}_{\mathbf{x}_s^{n-1}=\hat{\mathbf{x}}_{n-1}} = \begin{bmatrix} \cos(2\pi d \widehat{A}_l^{n-1}) & \sin(2\pi d \widehat{A}_l^{n-1}) \\ -\sin(2\pi d \widehat{A}_l^{n-1}) & \cos(2\pi d \widehat{A}_l^{n-1}) \end{bmatrix} \tag{16}$$

$$\boldsymbol{\beta}_{2l} = \begin{bmatrix} \frac{\partial z_{2l-1}^n}{\partial z_{2l-1}^{n-1}} & \frac{\partial z_{2l-1}^n}{\partial z_{2l}^{n-1}} \\ \frac{\partial z_{2l}^n}{\partial z_{2l-1}^{n-1}} & \frac{\partial z_{2l}^n}{\partial z_{2l}^{n-1}} \end{bmatrix}_{\mathbf{x}_s^{n-1}=\hat{\mathbf{x}}_{n-1}} = \begin{bmatrix} \cos(2\pi d \widehat{B}_l^{n-1}) & \sin(2\pi d \widehat{B}_l^{n-1}) \\ -\sin(2\pi d \widehat{B}_l^{n-1}) & \cos(2\pi d \widehat{B}_l^{n-1}) \end{bmatrix} \tag{17}$$

$$\begin{aligned}\boldsymbol{\beta}_{3l} &= \begin{bmatrix} \frac{\partial x_{2l-1}^n}{\partial A_l^{n-1}} \\ \frac{\partial x_{2l}^n}{\partial A_l^{n-1}} \end{bmatrix}_{\mathbf{x}_s^{n-1}=\hat{\mathbf{x}}_{n-1}}\\ &= 2\pi d \begin{bmatrix} -\sin(2\pi d \widehat{A}_l^{n-1}) & \cos(2\pi d \widehat{A}_l^{n-1}) \\ -\cos(2\pi d \widehat{A}_l^{n-1}) & -\sin(2\pi d \widehat{A}_l^{n-1}) \end{bmatrix} \begin{bmatrix} \hat{x}_{2l-1}^{n-1} \\ \hat{x}_{2l}^{n-1} \end{bmatrix}\end{aligned} \tag{18}$$

$$\boldsymbol{\beta}_{4l} = \begin{bmatrix} \frac{\partial z_{2l-1}^n}{\partial B_l^{n-1}} \\ \frac{\partial z_{2l}^n}{\partial B_l^{n-1}} \end{bmatrix}_{\mathbf{x}_s^{n-1}=\hat{\mathbf{x}}_{n-1}} = 2\pi d \begin{bmatrix} -\sin(2\pi d \widehat{B}_l^{n-1}) & \cos(2\pi d \widehat{B}_l^{n-1}) \\ -\cos(2\pi d \widehat{B}_l^{n-1}) & -\sin(2\pi d \widehat{B}_l^{n-1}) \end{bmatrix} \begin{bmatrix} \hat{z}_{2l-1}^{n-1} \\ \hat{z}_{2l}^{n-1} \end{bmatrix} \tag{19}$$

4.2.2. Updating step

The posterior estimates are updated depending on the difference between the estimated measurements $\mathbf{H}\,\hat{\mathbf{x}}_n^-$ and the observed measurements at the nth elements $\mathbf{Y}_n$. The updating step follows the following equations as in [21]

$$\begin{aligned}\mathbf{K}_n &= \mathbf{P}_n^- \mathbf{H}^T (\mathbf{R} + \mathbf{H}\,\mathbf{P}_n^-\,\mathbf{H}^T)^{-1}\\ \hat{\mathbf{x}}_n &= \hat{\mathbf{x}}_n^- + \mathbf{K}_n (\mathbf{Y}_n - \mathbf{H}\,\hat{\mathbf{x}}_n^-)\\ \mathbf{P}_n &= \mathbf{P}_n^- - \mathbf{K}_n\,\mathbf{H}\,\mathbf{P}_n^-\end{aligned} \tag{20}$$

where $\mathbf{K}_n$ is Kalman gain. The matrix $\mathbf{H}$ can be deduced by comparing both Eqs. (11) and (12). When the filter converges, the parameters θ_l and λ_l, with $l = 1,2...L$, can be then evaluated as

$$\begin{aligned}\theta_l &= \tan^{-1}\left(\frac{B_l}{A_l}\right)\\ \lambda_l &= \frac{\sin\theta_l}{A_l} \quad or \quad \lambda_l = \frac{\cos\theta_l}{B_l}\end{aligned} \tag{21}$$

4.3. Proposed unscented Kalman filter-based approach

In UKF, Gaussian-distributed state variable is represented by a minimal set of carefully chosen sample points, called sigma points. Sigma points capture both the mean and covariance of the state variable. Then, sigma points are propagated through nonlinear system. The system outputs corresponding to sigma points are used to perfectly recover Gaussian state variable. The state variable $\mathbf{x}_s$ can be estimated with UKF as well from the state space model in Eq. (7). UKF algorithm is first introduced in [22] that gives a clear derivation of the algorithm. First, UKF is initialized with $\hat{\mathbf{x}}_0^a$, a concatenation of the initial estimate $\hat{\mathbf{x}}_0$ and initial estimate of measurements noise. The initial covariance matrix $\mathbf{P}_0^a$ is initialized as well.

$$\begin{aligned}\hat{\mathbf{x}}_0^a &= [\hat{\mathbf{x}}_0^T \;\; 0]^T\\ \mathbf{P}_0^a &= \begin{bmatrix} \mathbf{P}_0 & 0 \\ 0 & \mathbf{P}_v \end{bmatrix}\end{aligned} \tag{22}$$

where $\mathbf{P}_0 = \mathrm{E}[(\mathbf{x}_s - \hat{\mathbf{x}}_0)(\mathbf{x}_s - \hat{\mathbf{x}}_0)^T]$ and $\mathbf{P}_v$ is the measurements noise covariance matrix (equivalent to $\mathbf{R}$ in EKF). Then, the filter repeats the following steps till it converges.

4.3.1. Selecting sigma points

For a state variable of dimension M, UKF selects 2M + 1 sigma points. Therefore, for 6L × 1 state variable $\mathbf{x}_s$, 12L + 1 sigma points are evaluated as follows.

$$\begin{aligned}\boldsymbol{\chi}_{0,n-1}^a &= \hat{\mathbf{x}}_{n-1}^a\\ \boldsymbol{\chi}_{i,n-1}^a &= \hat{\mathbf{x}}_{n-1}^a + (\sqrt{(6L+\Lambda)\mathbf{P}_{n-1}})_i, \quad i = 1,2...6L\\ \boldsymbol{\chi}_{i,n-1}^a &= \hat{\mathbf{x}}_{n-1}^a - (\sqrt{(6L+\Lambda)\mathbf{P}_{n-1}})_i, \quad i = 6L+1,...12L\end{aligned} \tag{23}$$

where Λ represents scaling parameter and $\Lambda = \alpha^2(6L + \kappa) - 6L$. The parameter α denotes the spread of sigma points around $\hat{\mathbf{x}}_n$ and κ is a secondary scaling parameter (usually 0). The term $(\sqrt{(6L+\Lambda)\mathbf{P}_{n-1}})_i$ represents the ith row of the matrix square root, evaluated by Cholesky decomposition.

4.3.2. Prediction step

Sigma points corresponding to the state variable only $\boldsymbol{\chi}_{i,n-1}^x$, with $i = 0,1,...12L$, are then propagated through the nonlinear process model to predict the posterior estimates $\hat{\mathbf{x}}_n^-$.

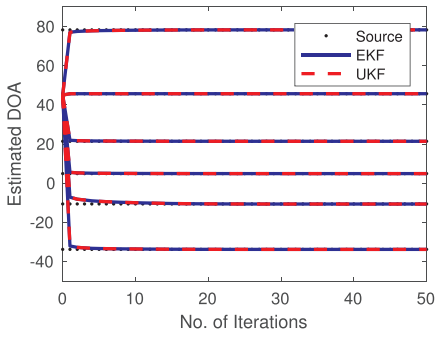

(a) Estimated DOA

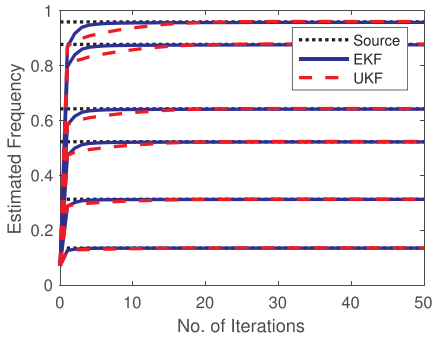

(b) Estimated N. frequency

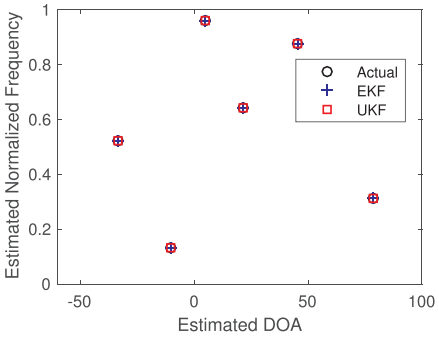

(c) Dual pairs

Fig. 1. Estimated parameters using EKF and UKF.

$$\chi^{x}_{i,n|n-1} = f(\chi^{x}_{i,n-1}) \tag{24}$$

where $f(.)$ is the nonlinear function that represents the process model shown in Eq. (7). The posterior estimate and covariance matrix are then evaluated as weighted mean and covariance of new sigma points.

$$\begin{aligned}\hat{\mathbf{x}}^{-}_{n} &= \textstyle\sum_{i=0}^{12L} w_i^{(m)}\, \chi^{x}_{i,n|n-1} \\ \mathbf{P}^{-}_{n} &= \textstyle\sum_{i=0}^{12L} w_i^{(c)}\, (\chi^{x}_{i,n|n-1}-\hat{\mathbf{x}}^{-}_{n})(\chi^{x}_{i,n|n-1}-\hat{\mathbf{x}}^{-}_{n})^{T}\end{aligned} \tag{25}$$

As in [22], the weights are evaluated in UKF algorithm as

$$\begin{aligned} w_0^{(m)} &= \frac{\Lambda}{6L+\Lambda} \\ w_0^{(c)} &= \frac{\Lambda}{6L+\Lambda} + (1-\alpha^2+\beta) \\ w_i^{(m)} &= w_i^{(c)} = \frac{1}{2(6L+\Lambda)}, \quad i = 0,1,\ldots 12L \end{aligned} \tag{26}$$

where β represents prior knowledge of the state distribution ($\beta = 2$ for Gaussian distribution). On the other hand, sigma points are propagated through measurements model to predict the posterior predicted measurements as well.

$$\begin{aligned}\mathbf{\Psi}_{i,n|n-1} &= \mathbf{H}\, \chi^{x}_{i,n|n-1} + \chi^{n}_{i,n|n-1} \\ \hat{\mathbf{y}}^{-}_{n} &= \textstyle\sum_{i=0}^{12L} w_i^{(m)}\, \mathbf{\Psi}_{i,n|n-1}\end{aligned} \tag{27}$$

4.3.3. Updating step

Like EKF, the posterior estimate and covariance are updated depending on the difference between observed measurements $\mathbf{Y}_n$ and the predicted measurements $\hat{\mathbf{y}}^{-}_{n}$ as follows.

$$\begin{aligned}\mathbf{K}_n &= \mathbf{P}_{\tilde{x}_n\tilde{y}_n}\, \mathbf{P}^{-1}_{\tilde{y}_n\tilde{y}_n} \\ \hat{\mathbf{x}}_n &= \hat{\mathbf{x}}^{-}_{n} + \mathbf{K}_n\, (\mathbf{Y}_n - \hat{\mathbf{y}}^{-}_{n}) \\ \mathbf{P}_n &= \mathbf{P}^{-}_{n} - \mathbf{K}_n\, \mathbf{P}_{\tilde{y}_n\tilde{y}_n}\, \mathbf{K}^{T}_{n}\end{aligned} \tag{28}$$

$$\begin{aligned}\mathbf{P}_{\tilde{y}_n\tilde{y}_n} &= \textstyle\sum_{i=0}^{12L} w_i^{(c)}\, (\mathbf{\Psi}_{i,n|n-1}-\hat{\mathbf{y}}^{-}_{n})(\mathbf{\Psi}_{i,n|n-1}-\hat{\mathbf{y}}^{-}_{n})^{T} \\ \mathbf{P}_{\tilde{x}_n\tilde{y}_n} &= \textstyle\sum_{i=0}^{12L} w_i^{(c)}\, (\chi^{x}_{i,n|n-1}-\hat{\mathbf{x}}^{-}_{n})(\mathbf{\Psi}_{i,n|n-1}-\hat{\mathbf{y}}^{-}_{n})^{T}\end{aligned} \tag{29}$$

When the filter converges, the parameters θ_l and λ_l can be estimated as in Eq. (22). Although UKF generally has better performance than EKF, it has to calculate a large number of sigma points in every iteration. As a result, UKF requires high time of processing.

5. Results and discussions

In this section, a numerical study is presented. The simulation model is first described, and then the results are discussed. Finally, a comparison among our proposal and proposals in [18,19] is presented.

5.1. Simulation model

For simulations, the number of elements in each array is set to 200 (N = 200) with inter-element spacing of one tenth of the minimum wavelength. Suppose that the two arrays receive signals from 6 different band-limited uncorrelated sources (L = 6). The normalized carrier frequencies of the received source signals are {0.878, 0.523, 0.643, 0.313, 0.135, 0.96} and their corresponding DOAs are {45.7, −33.8, 21.4, 78.3, −10.6, 4.9} respectively. In addition, signal to noise ratio (SNR) at the array elements is assumed to be 10 dB.

EKF and UKF are properly initialized and tuned to avoid filter divergence. In both filters, $\hat{\mathbf{x}}_0$ is preferably set around the mean value of $\mathbf{x}_s$. However, it is set to different values during simulations to examine and compare the performance of both two filters. On the other hand, $\mathbf{P}_0$ should be carefully assumed as a lower $\mathbf{P}_0$ than its true value leads the filter to trust bad estimates and neglect observed measurements. Thus, we set $\mathbf{P}_0$ to its true value through simulations. The last parameters to be tuned are $\mathbf{R}$ and $\mathbf{P}_v$ in EKF and UKF respectively. Noise variance in the arrays can be an indication for the value of $\mathbf{R}$ and $\mathbf{P}_v$, but they cannot be set to zero.

5.2. Simulation results

Monte-Carlo simulations have been executed over 500 snapshots for both EKF and UKF algorithms. First, the initial estimates were set to

value that is close to the mean of the state variable. So all the elements of $\hat{\mathbf{x}}_0$ were set to 0.05. Both EKF and UKF were able to efficiently detect all carrier frequencies and the corresponding DOA of all source signals. Fig. 1 shows the speed of convergence of both EKF and UKF. Both EKF and UKF need less than 10 iterations to converge to the true values of DOA as shown in Fig. 1a. However, EKF was faster than UKF in converging to the true values of carrier frequencies as shown in Fig. 1b. Since each iteration represents exploiting another array element, UKF needs more array elements than EKF to perfectly converge. As shown in Fig. 1c, both EKF and UKF succeeded to pair both carrier frequencies and their corresponding DOAs. According to simulations, EKF algorithm is 10 times faster than UKF. Although UKF is a derivative-free algorithm, it takes more time in evaluating the required sigma points in every iteration. Since the number of sigma points depends on the number of source signals, the processing time of UKF may increase exponentially with the increase in the number of source signals.

Another experiment has been executed to examine the effects of initial estimates. In this experiment, the initial estimates were set to 0.5 and 0.8. Then, the root mean square error (RMSE) in the estimated parameters has been evaluated over 500 snapshots. The results of all these cases are gathered in Fig. 2. When the initial estimate was set to 0.05 which is close to the mean value, both EKF and UKF gave the lowest RMSE in all cases. Then, RMSE tends to increase with the increase in the initial estimates. The reason of this degradation is the sub-optimality of EKF and UKF, and hence they may converge to a sub-optimal solution if they are not properly initialized.

To examine the effects of the inter-element spacing on the performance of EKF and UKF, the simulation was repeated with an inter-element spacing of one quarter of the minimum wavelength and an initial estimate of 0.05. Fig. 3 shows the difference between the two cases where the inter-element spacing was $\lambda_{min}/4$ and $\lambda_{min}/10$. In Fig. 3a where the inter-element spacing was $\lambda_{min}/10$, both EKF and UKF perfectly converged to the true values. When the inter-element spacing increased to one fourth of the minimum wavelength, the performance degraded as shown in Fig. 3b. In fact, the performance of EKF dramatically deteriorated compared to the performance of UKF because of the linearization errors. This proves the role of the inter-element spacing. When it decreases, the process state model expands to an extent in which it tends to be relatively linear regarding to the unknown state parameters. Thus, EKF starts to approach the performance of UKF as shown in Fig. 3a.

Our proposal can detect a number of source signals up to the number of the elements in a single ULA of the employed array. Thus, the structure used in these simulations was able to detect up to 199 sources. Since SUs have no prior information about PUs, spectrum sensing techniques should be blind. In this case, our proposal should be set to detect the maximum possible number of sources (L = 199). When the filter converges to the true values, the actual number of sources can be detected easily as the remaining signals would be converged to zero indicating their absence.

5.3. Comparative study

For the sake of comparison, Kumar and See [18] and Arianandа and Leus [19] are considered. These two algorithms depend on sub-Nyquist sampling and have employed different array structures with a large number of ADCs to achieve sub-Nyquist rates. Table 1 shows the differences in degrees of freedom, sampling rate and the number of employed ADCs among them and our proposal. Arianandа and Leus [19] has the highest degrees of freedom among the three algorithms. Since the increase in the number of the virtual elements N_s is faster than the increase in the number of the actual array elements N, Arianandа and Leus [19] can detect a large number of source signals with a few number of array elements [23]. For example, Arianandа and Leus [19] has degrees of freedom of more than 250 using 20 array elements only. However, Kumar and See [18] and our proposal can result in degrees of freedom of 24 and 9 respectively using the same number of array elements. Kumar and See [18] has the second highest degrees of freedom, which increase in a quadrature manner. As a result, when the number of array elements exceeds 13, the algorithm starts to detect a number of source signals higher than the employed array elements. However, our proposal has the lowest degrees of freedom, which increase linearly and cannot exceed the number of array elements as it depends on a dense array.

On the other hand, our proposal has the simplest hardware complexity since a single time sample is required. Since our proposal exploits the spatial domain, there is no restrictions on the sampling rates. Then, a number of ADCs equal to the number of array elements are sufficient to capture one time sample. However, the other algorithms relying on sub-Nyquist rates require a large number of relaxed ADCs, which have restricted minimum sampling rates. Kumar and See [18] requires a number of ADCs equal to 1.5 times the number of array element. Thus, it has the second simplest hardware. However, Arianandа and Leus [19] requires a number of ADCs depending on N_s. Since the ratio N/N_s decreases with the increase in N, it results in an increasing number of ADCs and a more complex hardware architecture for larger problems.

6. Conclusions

The problem of jointly estimating DOA and carrier frequency of uncorrelated band-limited source signals can improve the capacity of SUs in CR. In this paper, both EKF and UKF are proposed for handling this

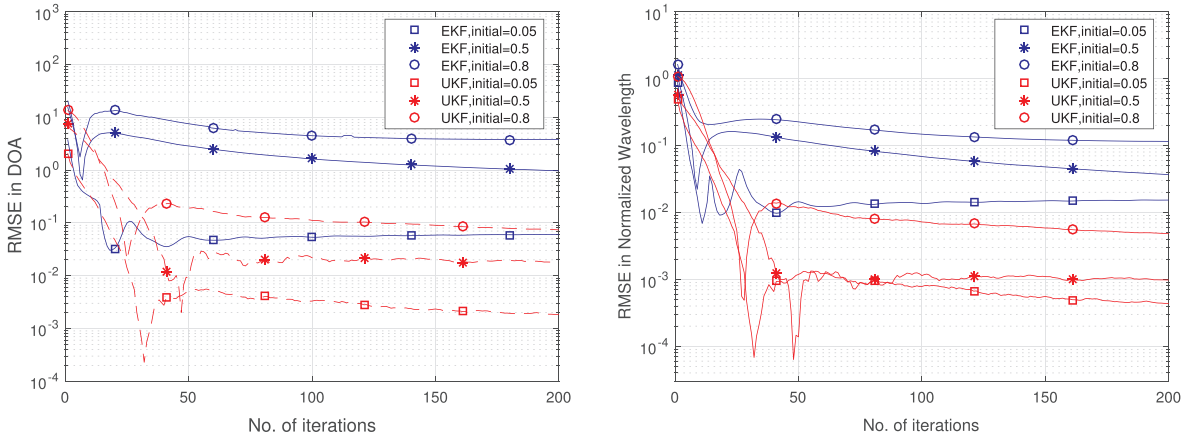

(a) RMSE in DOA (b) RMSE in n. wavelength

Fig. 2. RMSE in the estimated parameters with different initial estimates.

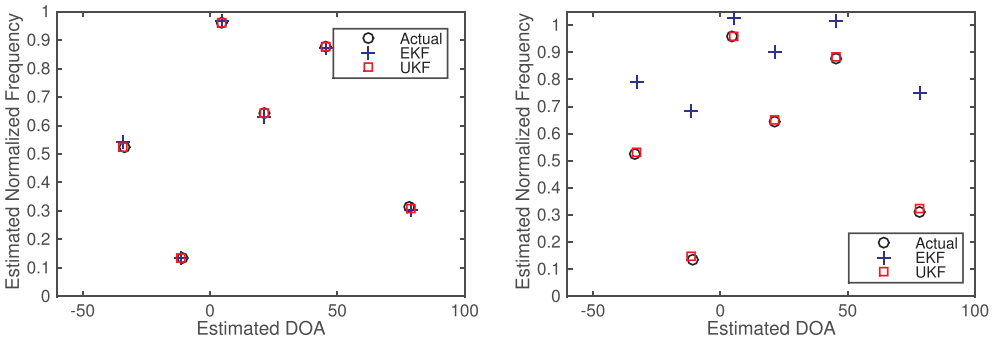

(a) $d = \lambda_{min}/10$ (b) $d = \lambda_{min}/4$

Fig. 3. Estimated DOA and carrier frequencies at different inter-element spacing.

Table 1
Comparison among our proposal and some related work.

	Arianandа and Leus [19]	Kumar and See [18]	KF-based proposed approaches
Discussion	Reconstructed power spectrum is a predefined grid where estimated parameters are approximated to the nearest values	It gives precise estimation since estimated parameters are evaluated numerically	Like [18], estimated parameters are evaluated numerically leading to precise estimations
Degrees of freedom	$2N_s-1$ for an N activated elements in an N_s virtual ULA	Wideband spectrum is completly reconstructed $\left\lceil \frac{N}{4} \right\rceil^2 - 1$ for a 2D nested array with N elements	Spectrum cannot be reconstructed since the system consider a single sample N−1 for an (2N − 1) L-shaped uniform array
Minimum sampling rate	N_sM_sB[a]	$\frac{(3N+1)B}{2}$	No restrictions
No. of ADCs employed	N_sM_s	$\frac{(3N+1)}{2}$	2N−1

[a] M_s denotes number of channels of multi-coset sampler and B denotes bandwidth of band-limited source signals.

problem. The proposed approaches employ an L-shaped array antenna with inter-element spacing less than or equal one half of the minimum wavelength. To relax ADC requirements, EKF and UKF are applied on the spatial domain. Simulations prove that both EKF and UKF can jointly detect the DOAs and carrier frequencies of PUs, however UKF shows a better performance. From simulations, it was obvious that the initial estimates, inter-element spacing and filter tuning can enhance the filter performance. In comparison to the related work in the literature, our approaches decrease hardware complexity. The reason is that the proposed approaches depend on one time sample and detect parameters from the spatial domain without spectrum reconstruction. However, the number of source signals that can be detected is restricted to the number of array elements leading to lower degrees of freedom.

References

[1] Mitola J, Maguire GQ. Cognitive radio: making software radios more personal. IEEE Pers Commun 1999;6(4):13–8.
[2] Ren X, Chen C. Spectrum sensing algorithm based on sample variance in multi-antenna cognitive radio systems. Int J Electron Commun AEU 2016;70(12):1601–9.
[3] Qing H, Li H, Chu N, Liu G, Liu Y. Multistage Wiener filter aided MDL approach for wideband spectrum sensing in cognitive radio networks. Int J Electron Commun AEU 2017;73(March):165–72.
[4] Sun F, Wu Q, Sun Y, Ding G, Lan P. An iterative approach for sparse direction-of-arrival estimation in co-prime arrays with off-grid targets. Digit Signal Process 2017;61:35–42.
[5] Liu A, Yang Q, Zhang X, Deng W. Direction-of-arrival estimation for coprime array using compressive sensing based array interpolation. Int J Antennas Propag 2017;2017(February):1–10.
[6] Alinezhad P, Seydnejad SR, Abbasi-Moghadam D. DOA estimation in conformal arrays based on the nested array principles. Digit Signal Process 2016;50(C):191–202.
[7] Qin S, Zhang YD, Amin MG. Generalized coprime array configurations for direction-of-arrival estimation. IEEE Trans Signal Process 2015;63(6):1377–90.
[8] Xiaofei Z, Jianfeng L, Lingyun X. Novel two-dimensional DOA estimation with L-shaped array. J Adv Signal Process EURASIP 2011;2011(1):50.
[9] Wu Q, Sun F, Lan P, Ding G, Zhang X. Two-dimensional direction-of-arrival estimation for co-prime planar arrays: a partial spectral search approach. IEEE Sens J 2016;16(14):5660–70.
[10] Qian C, Huang L, Shi Y, So HC. Joint angle and frequency estimation using structured least squares. Proc IEEE Int Conf Acoust Speech Signal Process 2014:p–6.
[11] Lemma AN, van der Veen AJ, Deprettere EF. Joint angle-frequency estimation using multi-resolution ESPRIT. Proc IEEE Int Conf Acoust Speech Signal Process 1998;4:1957–60.
[12] Xudong W, Zhang X, Li J, Bai J. Improved ESPRIT method for joint direction-of-arrival and frequency estimation using multiple-delay output. Int J Antennas Propag 2012;2012:1–9.
[13] Kumar AA, Razul SG, See CMS. An efficient sub-Nyquist receiver architecture for spectrum blind reconstruction and direction of arrival estimation. Proc IEEE Int Conf Acoust Speech Signal Process 2014:6781–5.
[14] Kumar AA, Razul SG, See CMS. Spectrum blind reconstruction and direction of arrival estimation at sub-Nyquist sampling rates with uniform linear array. IEEE Int Conf Digit Signal Process 2015:670–4.
[15] Kumar AA, Razul SG, See CMS. Spectrum blind reconstruction and direction of arrival estimation of multi-band signals at sub-Nyquist sampling rates. Multidimens Syst Signal Process. September 2016. p. 1–27.
[16] Roy R, Kailath T. ESPRIT-estimation of signal parameters via rotational invariance techniques. IEEE Trans Acoust Speech Signal Process 1989;37(7):984–95.
[17] Schmidt R. Multiple emitter location and signal parameter estimation. IEEE Trans Antenn Propag 1986;34(3):276–80.
[18] Kumar AA, Razul SG, See CMS. Carrier frequency and direction of arrival estimation with nested sub-Nyquist sensor array receiver. Proc Eur signal process conf EUSIPCO. 2015. p. 1167–71.
[19] Arianandа DD, Leus G. Compressive joint angular-frequency power spectrum estimation for correlated sources. Proc Eur signal process conf EUSIPCO. 2013. p. 1–5.
[20] Kumar AA, Chandra MG, Balamuralidhar P. Joint frequency and 2-D DOA recovery with sub-Nyquist difference space-time array. Proc Eur signal process conf EUSIPCO. 2017. p. 420–4.
[21] G. Welch, G. Bishop, An Introduction to the Kalman Filter, 2006, p. 16.
[22] Julier SJ, Uhlmann JK. New extension of the Kalman filter to nonlinear systems. Proc SPIE 1997;3068:182–93.
[23] Arianandа DD, Leus G. Compressive wideband power spectrum estimation. IEEE Trans Signal Process 2012;60(9):4775–89.